Preparation and Characterization of Highly Ordered Graphitic Mesoporous Carbon as a Pt Catalyst Support for Direct Methanol Fuel Cells

Fabing Su, Jianhuang Zeng, Xiaoying Bao, Yaoshan Yu, Jim Yang Lee, and X. S. Zhao*

Department of Chemical and Biomolecular Engineering, National University of Singapore, 10 Kent Ridge Crescent, Singapore 119260

Received January 31, 2005. Revised Manuscript Received May 25, 2005

Mesoporous carbon with graphitic pore walls is highly desired in many electrochemical applications such as fuel cells and lithium ion batteries. In this study, ordered graphitic mesoporous carbon was prepared by chemical vapor deposition (CVD) of benzene in the pores of mesoporous SBA-15 pure-silica template without loading any catalytic species. Nitrogen adsorption, small-angle X-ray scattering, X-ray diffraction, Raman spectrometry, field-emission scanning electron microscopy, transmission electron microscopy, and thermogravimetric analysis techniques were used to characterize the samples. It was observed that the CVD method affords highly ordered mesoporous carbon with graphitic pore walls and low carbon shrinkage because of the high degree of infiltration of pyrolytic carbon. The catalytic performance of the mesoporous carbon as a support for Pt catalyst in room-temperature methanol oxidation was examined. Results show that the specific activity of the Pt catalyst supported on the mesoporous carbon is higher than that of a commercial Pt catalyst form E-TEK.

1. Introduction

The preparation of ordered mesoporous carbons using ordered mesoporous materials as the templates has been of recent great research interest.[1−4] These carbon materials can be used as catalyst supports,[5] electrode materials,[6] adsorbents,[7] and templating matrixes for fabricating nanostructures[8] because of their prominent characteristics, such as high surface area, relatively uniform pore size, ordered pore structure, interconnected pore network, tailorable surface properties, and good thermal and mechanical stabilities. The electrochemical properties of a porous carbon used as an electrode in direct-methanol fuel cells (DMFCs),[9] electrochemical double-layer capacitors,[10] and lithium ion batteries,[6] have been found to be closely related to its graphitic nature. Therefore, preparation of ordered mesoporous carbon with graphitic pore walls is of importance. To prepare ordered graphitic mesoporous carbons, some unconventional carbon precursors such as mesophase pitch,[10] acenaphthene,[11] polyvinyl chloride,[12] naphthalene, anthracene, pyrene,[13] and polypyrrole[14] have been employed to infiltrate the pores of mesoporous templates. However, infiltration and polymerization using these liquid carbon precursors are time consuming because repeated infiltration and polymerization are required in order to obtain an ordered carbon replica. On the other hand, polymerization and pyrolysis of the carbon precursors during high-temperature carbonization often lead to the emission of a large amount of small molecules such as H_2O, which can deteriorate the pore structure of the templates,[15] thus the structural ordering of the resultant carbon.[16,17]

CVD method, which is a well-established technique for preparing carbon molecular sieves,[18] carbon nanofibers,[19] and carbon nanotubes,[20] has a number of advantages over the liquid-phase impregnation method, such as a high degree of pore filling,[21] easy control over the amount of pyrolytic carbon deposited in the template pores,[17] enabling the

* To whom correspondence should be addressed. Tel: +65-68744727. Fax: +65-67791936. E-mail: chezxs@nus.edu.sg.

(1) Ryoo, R.; Joo, S. H.; Kruk, M.; Jaroniec, M. *Adv. Mater.* **2001**, *13*, 677.
(2) Schüth, F. *Adv. Mater.* 2003, *42*, 3604.
(3) Lee, J.; Han, S.; Hyeon, T. *J. Mater. Chem.* **2004**, *14*, 478.
(4) Yang, H.; Zhao, D. *J. Mater. Chem.* **2005**, *15*, 1217.
(5) Joo, S. H.; Choi, S. J.; Oh, I.; Kwak, J.; Liu, Z.; Terasaki, O.; Ryoo, R. *Nature* **2001**, *412*, 169.
(6) Zhou, H.; Zhu, S.; Hibino, M.; Honma, I.; Ichihara, M. *Adv. Mater.* 2003, *15*, 2107.
(7) Hartmann, M.; A. Vinu, A.; Chandrasekar, G. *Chem. Mater.* **2005**, *17*, 829.
(8) Roggenbuck, J.; Tiemann, M. *J. Am. Chem. Soc.* **2005**, *127*, 1096.
(9) Hyeon, T.; Han, S.; Sung, Y. E.; Park, K. W.; Kim, Y. W. *Angew. Chem., Int. Ed.* 2003, *42*, 4352.
(10) Yang, H.; Yan, Y.; Liu, Y.; Zhang, F.; Zhang, R.; Meng, Y.; Li, M.; Xie, S.; Tu, B.; Zhao, D. *J. Phys. Chem. B* **2004**, *108*, 17320.
(11) Kim, T. W.; Park, I. S.; Ryoo, R. *Angew. Chem., Int. Ed.* **2003**, *42*, 4375.
(12) Fuertes, A. B.; Alvarez, S. *Carbon* **2004**, *42*, 3049.
(13) Kim, C. H.; Lee, D. K.; Pinnavaia, T. J. *Langmuir* **2004**, *20*, 5157.
(14) Yang, C. M.; Weidenthaler, C.; Spliethoff, B.; Mayanna, M.; Schüth, F. *Chem. Mater.* **2005**, *17*, 355.
(15) Zhang, F.; Yan, Y.; Yang, H.; Meng, Y.; Yu, C.; Tu, B.; Zhao, D.*J. Phys. Chem. B* **2005**, *109*, 8723.
(16) Ehrburger-Dolle, F.; Morfin, I.; Geissler, E.; Bley, F.; Livet, F.; Vix-Guterl, C.; Saadallah, S.; Julien, P.; Reda, M.; Patarin, J.; Iliescu, M.; Werckmann, J. *Langmuir* **2003**, *19*, 4303.
(17) Parmentier, J.; Vix-Guterl, C.; Gibot, P.; Reda, M.; Ilescu, M.; Werckmann, J.; Patarin, J. *Microporous. Mesoporous. Mater.* **2003**, *62*, 87.
(18) Kawabuchi, Y.; Kishino, M.; Kawano, S.; Whitehurst, D. D.; Mochida, I. *Langmuir* **1996**, *12*, 4281.
(19) Zheng, G. B.; Kouda, K.; Sano, H.; Uchiyama, Y.; Shi, Y. F.; Quan, H. J. *Carbon* **2004**, *42*, 635.
(20) Hata, K.; Futaba, D. N.; Mizuno, K.; Namai, T.; Yumura, M.; Iijima, S. *Science* **2004**, *306*, 1362.
(21) Kyotani, T.; Ma, Z.; Tomita, A. *Carbon* **2003**, *41*, 1451.

10.1021/cm0502222 CCC: $30.25
Published on Web 06/29/2005

formation of graphitic pore walls,[22] and avoiding the formation of additional microporosity.[16] By use of the CVD method, Ryoo and co-workers prepared ordered mesoporous carbon (CMK-4) with $AlCl_3$-impreganted MCM-48 as the template and acetylene as the gaseous carbon precursor.[23] Zhang et al.[24] employed catalytic CVD (CCVD) to prepare ordered mesoporous carbon with Co-loaded SBA-15 as the template and ethylene as the carbon precursor. Pinnavaia and co-workers utilized a MSU−H template containing Fe nanoparticles to fabricate a highly conductive mesoporous carbon using the CVD technique.[13]

The use of a mesoporous pure silica template without loading any catalyst is practically important because of the elimination of the catalyst loading step. Vix-Guterl et al.[25] first described the use of pure silica MCM-48 as the template to fabricate ordered mesoporous carbon. Subsequently, Xia and co-workers[22,26,27] reported the preparation and characterization of ordered mesoporous carbon materials of various morphologies and structural types using SBA-15 silica template. To create graphitic pore walls, the authors employed the CVD method with styrene and acetonitrile as the carbon precursors. However, the morphology of the replicated carbon particles was observed to be different from that of the SBA-15 template when CVD temperature was higher than 900 °C.[22,26,27]

In the present work, large-pore SBA-15 pure silica was used as the template and benzene was employed as the carbon precursor to prepare ordered mesoporous graphitic carbon. The carbon materials were used as Pt catalyst supports for room-temperature methanol oxidation. It was observed that gaseous benzene is a good carbon precursor for fabricating mesoporous carbons, affording a high degree of carbon infiltration. The mechanism of thermal deposition of benzene on the template surface was discussed. Pt catalyst supported on the template-synthesized mesoporous carbon was found to display a higher specific activity for methanol oxidation than a commercial catalyst, Pt/C (E-TEK), which is a Pt catalyst supported on carbon black Vulcan XC-72.

2. Experimental Section

2.1. Synthesis. Mesoporous SBA-15 pure-silica template was prepared following the method described by Zhao et al.[28] Surfactant P123 was removed by calcination at 550 °C for 6 h with a heating rate of 2 °C/min in air. To investigate the change of pore structure of the silica under the thermal conditions of CVD of benzene employed in this work, a template-free SBA-15 silica sample was heated at 900 °C for 2 h with a heating rate of 5 °C/min under highly pure N_2 flow (30 cm^3/ min). The sample thus obtained is donated as SBA-15N.

The preparation of graphitic mesoporous carbons is described as follows. Around 0.3 g of pure-silica SBA-15 template was placed in a crucible and loaded in a horizontal quartz tube equipped with a furnace. The template was then heated to 900 °C in highly pure N_2 flow (30 cm^3/min) with a heating rate of 5 °C/min. Subsequently, N_2 flow (30 cm^3/min) containing 12 wt % benzene vapor from a liquid bubbler was passed through the quartz tube. After the CVD reaction of benzene occurred at 900 °C for 1h, the sample was cooled in pure nitrogen to obtain a template/carbon composite. The silica template was removed using a 46% HF solution at room temperature for 24 h, followed by washing with copious deionized water and drying in air at 150 °C for 5 h to yield a carbon sample, denoted as C-1. Another carbon sample prepared similarly, named C-2, was obtained when the CVD time was prolonged to 2 h at 900 °C.

2.2. Characterization. The pore properties of the SBA-15 silica and carbon samples were investigated using physical adsorption of nitrogen at the liquid-nitrogen temperature (−196 °C) on an automatic volumetric sorption analyzer (Quantachrome, NOVA1200). Prior to measurements, the samples were degassed at 200 °C for 5 h under vacuum. The specific surface areas were determined according to the Brunauer−Emmett−Teller (BET) method in the relative pressure range of 0.05−0.2. The total pore volumes were obtained from the volume of nitrogen adsorbed at the relative pressure of 0.99. Pore size distribution (PSD) curves were derived from the Barrett−Joyner−Halenda (BJH) method using the adsorption branches. The pore sizes were estimated from the maximum positions of the BJH PSD curves. The mesostructures of both the template and the carbon samples were characterized using small-angle X-ray scattering (SAXS) technique on a Bruker NanoStar with Cu Kα radiation of wavelength $\lambda = 0.15418$ nm. The graphitic nature of the mesoporous carbon samples was characterized using X-ray diffraction (XRD) technique (XRD-6000, Shimadzu, Japan) with Cu Kα radiation of wavelength $\lambda = 0.15418$ nm. Raman spectra were recoded on a Jobin-Yavon T6400 micro-Raman system at room temperature with an argon-ion laser at an excitation wavelength of 514.5 nm. Thermogravimetric analysis (TGA) was conducted on a thermogravimetric analyzer TGA 2050 (Thermal Analysis Instruments, USA) in air with a flow rate of 100 mL/min. The microscopic features of the samples were observed with a field-emission scanning electron microscope (FESEM) (JSM-6700F, JEOL Japan) operated at 10 kV, transmission electron microscopy (TEM) (JEM 2010, JEOL, Japan) operated at 200 kV, and field-emission transmission electron microscopy (FETEM) (JEM 2010F, JEOL, Japan) operated at 200 kV. A Perkin-Elmer 2400 Series II CHNS/O analyzer was used for elemental analysis.

2.3. Preparation and Electrochemical Evaluation of Pt Catalysts. Pt catalysts supported on carbons C-1 and C-2, which were designed as Pt/C-1 and Pt/C-2, respectively, were prepared using the borohydride reduction method as described elsewhere.[29] Briefly, 0.05 M chloroplatinic acid ($H_2PtCl_6 \cdot 6H_2O$, Aldrich) solution was added in distilled water containing carbon powder under stirring. Then, a 0.5 M excess of $NaBH_4$ (Aldrich) solution was used to initiate deposition of Pt nanoparticles. After stirring for 12 h, the solid was recovered by centrifugation, extensively washed with distilled water, and vacuum dried at room temperature overnight. The Pt loading was controlled to be 20 wt % to allow a fair comparison with a commercial Pt catalyst supported on carbon black Vulcan XC-72 with a specific surface area of 220 m^2/g from E-TEK, herein named as Pt/C (E-TEK), which also has a Pt loading of 20 wt %. A three-compartment electrochemical cell was used to evaluate the electrochemical performances of the catalysts by

(22) Xia, Y.; Mokaya, R. *Adv. Mater.* **2004**, *16*, 1553.
(23) Kaneda, M.; Tsubakiyama, T.; Carlsson, A.; Sakamoto, Y.; Ohsuna, T.; Terasaki, O.; Joo, S. H.; Ryoo, R. *J. Phys. Chem. B* **2002**, *106*, 1256.
(24) Zhang, W. H.; Liang, C.; Sun, H.; Shen, Z.; Guan, Y.; Ying, P.; Li, C. *Adv. Mater.* 2002, *14*, 1776.
(25) Vix-Guterl, C.; Boulard, S.; Parmentier, J.; Werckmann, J.; Patarin, J. *Chem. Lett.* **2002**, *10*, 1062.
(26) Xia, Y.; Mokaya, R. *Adv. Mater.* **2004**, *16*, 886.
(27) Xia, Y.; Yang, Z.; Mokaya, R. *J. Phys. Chem. B* **2004**, *108*, 19293.
(28) Zhao, D.; Feng, J.; Huo, Q.; Melosh, N.; Fredrickson, G. H.; Chmelka, B. F.; Stucky, G. D. *Science* **1998**, *279*, 548.
(29) Zeng, J.; Lee, J. Y. *J. Power Sources* **2004**, *140*, 268.

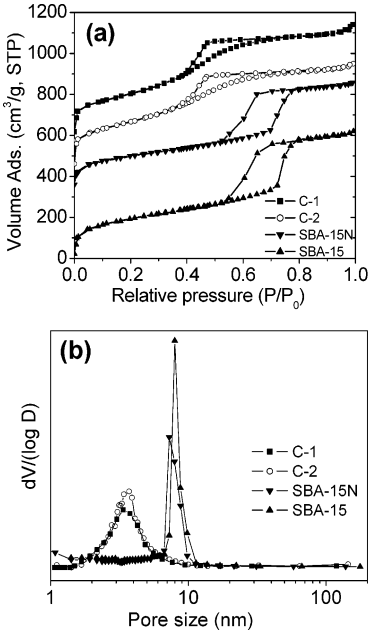

Figure 1. (a) Adsorption−desorption isotherms and (b) BJH−PSD curves of SBA-15 silicas and mesoporous carbons (for clarity, the isotherms of SBA-15N, C-1, and C-2 were vertically shifted for 350, 600, and 450 cm^3/g, respectively).

cyclic voltammetry at room temperature. An Autolab PGSTAT12 was used as a potentiostat/galvansotat. The working electrode was fabricated by casting Nafion-impregnated catalyst ink onto a 5 mm diameter vitreous glassy carbon disk electrode. A Pt gauze and a saturated calomel electrode (SCE) were used as the counter and the reference electrodes, respectively, and 0.5 M H_2SO_4 with or without 1 M CH_3OH were the electrolytes. All reported potentials were referenced to the SCE. The catalysts were electrochemically cleaned by continuous cycling until a stable response was obtained before the cyclic voltammograms were recorded. The electrochemically active surface areas of the Pt catalysts were estimated from the charges associated with hydrogen adsorption on Pt in the potential range of −0.2−0.1 V. The baseline of the measurement was extended from the double-layer region of each cyclic voltammogram (CV). The electrochemical surface area in cm^2 was calculated assuming a correspondence value of 0.21 mC/cm^2 Pt.[30]

3. Results and Discussion

3.1. Nitrogen Adsorption/Desorption Isotherms. Figure 1 shows the N_2 adsorption−desorption isotherms and BJH PSD curves of the SBA-15 silica template before and after thermal treatment at 900 °C for 2 h, as well as carbons C-1 and C-2 replicated from the template. The BET surface areas and pore parameters of the samples determined from the adsorption data are summarized in Table 1.

It is seen from Figure 1a that samples SBA-15 and SBA-15N display a type-IV isotherm with an H1 hysteresis loop, indicating they are mesoporous materials with cylindrical pore channels.[28,31] Capillary condensations of nitrogen in the relative pressure range of 0.7−0.8 can be seen from the adsorption branches, demonstrating the presence of relatively uniform mesopores. Upon heat treatment in nitrogen at 900 °C for 2 h, the maximum position of the BJH PSD peak (see Figure 1b) was slightly shifted from 7.9 to 7.2 nm. Accordingly, the surface area and pore volume (see Table 1) were slightly decreased due to the slight shrinkage of the silica framework.[32] Therefore, it can be concluded that the pore structure of the SBA-15 silica template was well preserved after thermal treatment at 900 °C for 2 h. As observed previously,[22] a low CVD temperature can hardly create graphitic carbon pore walls. This conclusion was also confirmed in this study (at a CVD temperature of 800 °C, no graphitic carbon was observed). On the other hand, a high CVD temperature may cause structural collapses of SBA-15 silica,[16,32] especially the ordered pore structure may totally collapse at 1100 °C. Therefore, a CVD temperature of 900 °C was employed in this work.

The nitrogen adsorption-desorption isotherms of carbons C-1 and C-2 also reveal a type-IV isotherm with a H2 hysteresis loop,[31] again indicating they are mesoporous materials. But, the capillary condensation steps in both samples are poorly defined, mostly probably due to the inverse replicated structures, in which the carbon nanorods were replicated from the pore channels of the mesoporous template. Thus, the peaks of the PSD curves of both carbons are substantially broader than those of the mesoporous silicas (see Figure 1b). The similarity between C-1 and C-2 in nitrogen isotherm and the PSD curve indicates both carbons possess a similar pore structure. The slightly lower surface area, pore volume, and pore size of C-2 than that of C-1 may suggest that the CVD time of 2 h brought about more carbon into the pore channels or on the external surface of silica template. On the other hand, the surface area and pore volume of both carbon samples are lower than that of an amorphous mesoporous carbon, CMK-3, which was synthesized using sucrose as the carbon precursor,[33] but slightly

Table 1. Texture Parameters of SBA-15 Templates and Mesoporous Carbons

sample	S_{BET}[a] (cm^3/g)	V_t[b] (cm^3/g)	w[c] (nm)	d_{100}[d] (nm)
SBA-15	699	0.95	7.9	10.8
SBA-15N	543	0.78	7.2	10.0
C-1	743	0.86	3.7	10.0
C-2	676	0.72	3.4	9.8
CMK-3[e]	1520	1.30	4.5	8.4

[a] BET surface area. [b] Total pore volume. [c] Pore diameter derived from BJH method. [d] (100) interplanar distance calculated using $d_{100} = \lambda/(2 \sin \theta)$. [e] From ref 33.

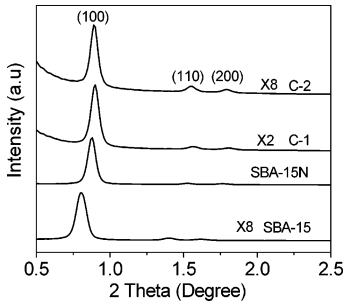

Figure 2. SAXS patterns of mesoporous SBA-15 silicas and carbons.

(30) Jose, M.; Rodriguez, D.; Herrera, J. A.; Pena, J. P. *J. Chem. Educ.* **2000**, *77*, 1195.
(31) Sing, K. S. W.; Everett, D. H.; Haul, R. A. W.; Moscou, L.; Pierotti, R. A.; Rouquerol, J, Siemieniewska, T. *Pure. Appl. Chem.* **1985**, *57*, 603.
(32) Matos, J. R.; Mercuri, L. P.; Kruk, M.; Jaroniec, M. *Chem. Mater.* **2001,** *13*, 1726.

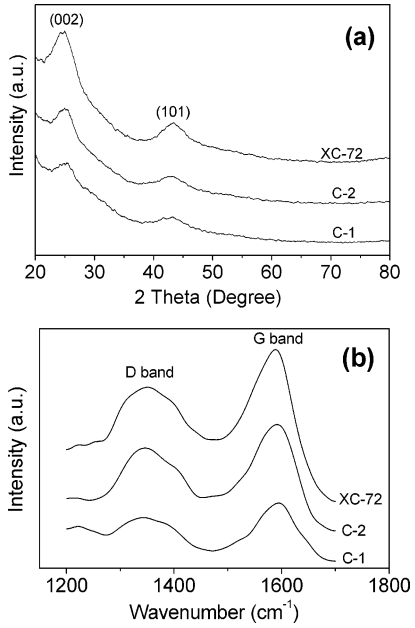

Figure 3. XRD patterns (a) and Raman spectra (b) of mesoporous carbons and carbon black XC-72.

higher than that of the graphitic mesoporous carbons prepared with mesophase pitch.[10] It is well known that the mesopores of amorphous carbon CMK-3 originated from the framework of the template, whereas micropores, which contributed significantly to the porosity, were created due to the emission of small molecules from the carbon precursor. With the CVD method, however, pyrolytic carbon is filled into the pores of the mesoporous silica template and the resultant carbon pore walls after template removal consist of stacked graphene layers, which are denser than amorphous carbon. Thus, both C-1 and C-2 have a smaller specific surface area and a lower pore volume than CMK-3.

3.2. SAXS Patterns. Figure 2 shows the SAXS patterns of the template and carbon samples. The SBA-15 silica template displays well-resolved (100), (110), and (200) peaks, demonstrating the presence of ordered 2D hexagonal pore arrays.[28,33] After thermal treatment at 900 °C for 2 h under nitrogen flow, the (100) peak was slightly shifted from 0.80 to 0.88° 2θ, thus the interplanar distance d_{100} was changed from 10.8 to 10.0 nm (see Table 1), implying a slight structural shrinkage upon high-temperature thermal treatment, in agreement with the nitrogen adsorption data in Figure 1. The SAXS patterns of carbons C-1 and C-2 show the presence of the (100), (110), and (200) diffractions, indicating a highly ordered 2D hexagonal mesostructure. Here it is worthy to note that the (100) peak positions of carbons C-1 and C-2 are very close to that of sample SBA-15N (0.88°). In addition, the presence of the well-resolved (110) and (200) peaks on both carbons, which are an indication of long-range structural ordering,[28] implies a complete replication process of the carbons without an obvious shrinkage from the SBA-15 silica template.

3.3. XRD Patterns and Raman Spectra. Figure 3a compares the wide-angle XRD patterns of carbons C-1 and C-2 with carbon black XC-72. Two diffraction peaks located at around 25 and 43°, corresponding to (002) and (101) diffractions of graphitic carbon,[10,11,22] can be seen on all samples. The intensities of the two peaks of carbons C-1 and C-2 are lower than that of XC-72, showing a poorer graphitic crystallinity of the carbon samples prepared in this work than XC-72. It is also seen that the intensity of the reflection peaks of carbon C-2 is slightly higher than that of

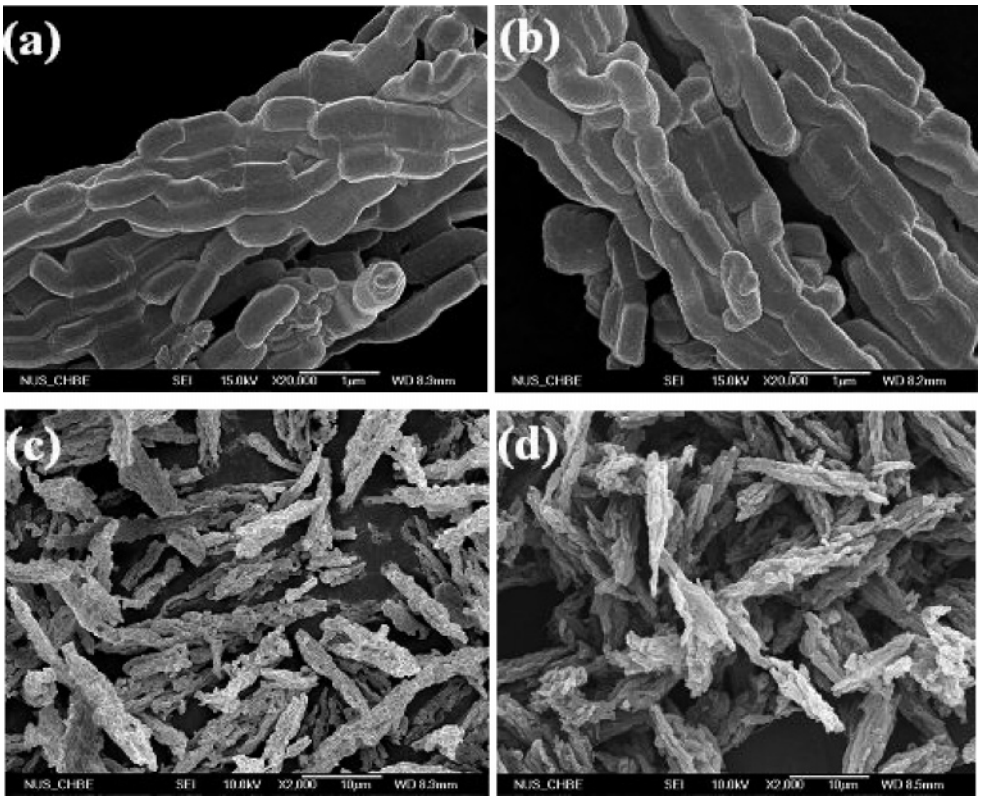

Figure 4. FESEM images of SBA-15 silica (a, c) and carbon C-2 (b, d).

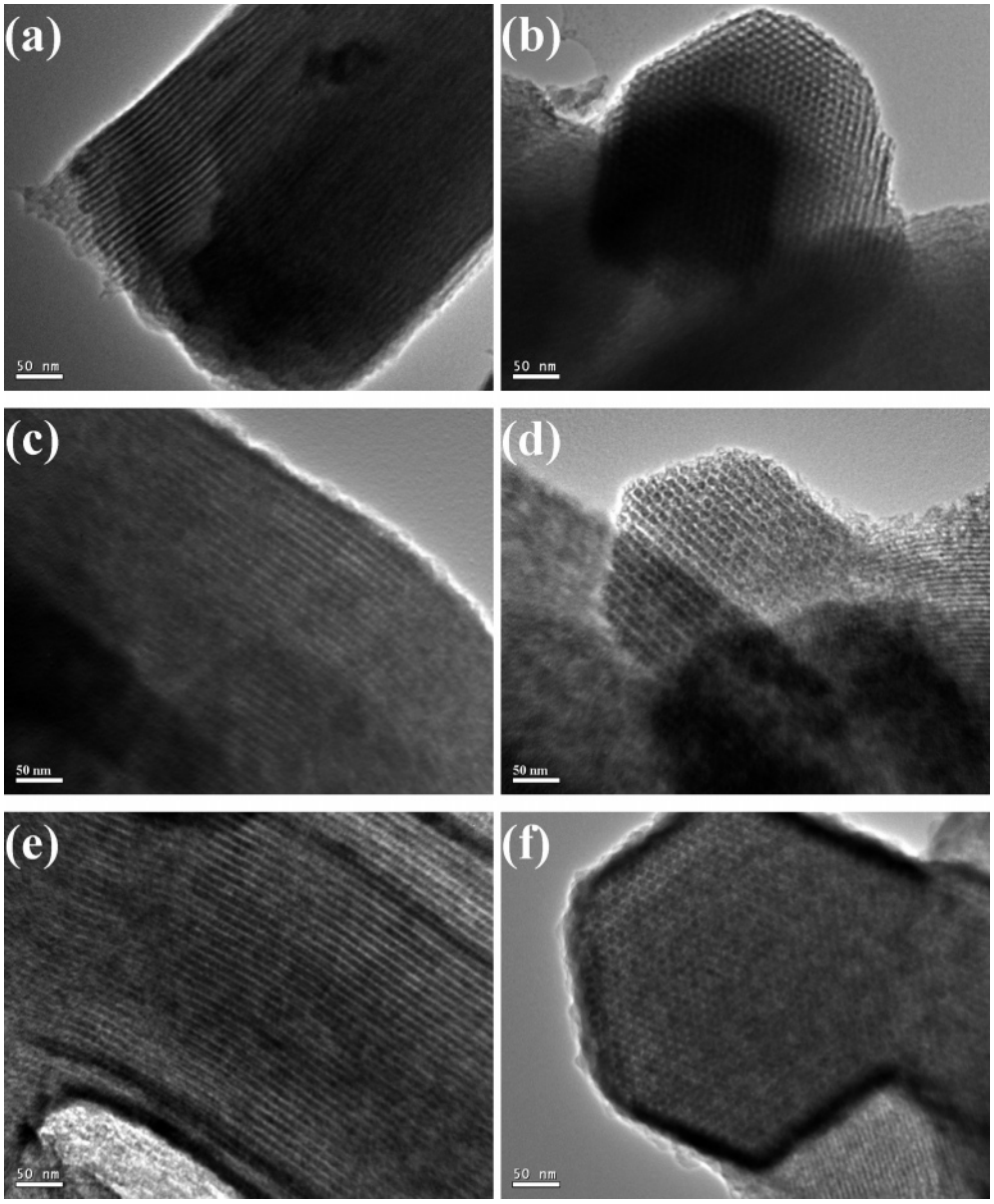

Figure 5. TEM images of silica SBA-15N (a, b), carbon C-1 (c, d), and carbon C-2 (e, f).

carbon C-1, indicating that the former contains slightly more graphitic carbon than the latter. In addition, no peaks at 53° and 78° corresponding to the (004) and (110) diffractions can be seen, implying that the carbon samples prepared in this work have a lower crystallinity than the graphitic porous carbon prepared with polyaromatic compound as the carbon precursor.[11]

Figure 3b shows the Raman spectra of different carbons, in which a strong peak at about 1580 cm^{-1} and a weak peak at 1350 cm^{-1} can be clearly seen. The peak at 1580 cm^{-1} (G band) is attributed to the vibration of sp^2-bonded carbon atoms in a 2D hexagonal lattice, namely, the stretching modes of C═C bonds of typical graphite, while the peak at 1350 cm^{-1} (D band) is associated with vibrations of carbon atoms with dangling bonds in plane terminations of the disordered graphite and related to the defects and disorders in structures in carbon materials. Graphite single crystals always exhibit a high-intensity sharp G-band at around 1580 cm^{-1}. The relative intensities of these two lines depend on the type of graphitic materials and reflect the graphitization degree. For these three carbons, the broad peak with a low intensity at 1350 cm^{-1} (D band) and the narrow peak with a high intensity at 1580 cm^{-1} (G band) indicate that the carbons were possibly composed of small graphite sheets with a low graphitization degree,[34] while the degree of C-2 is roughly lower than XC-72 and higher than C-1. These results agree well with the XRD data presented in Figure 3a, in which the difference of the peak at around 25° representing (002) plane of graphite can be seen.

3.4. FESEM Observation. Figure 4 shows the FESEM images of the SBA-15 silica template and mesoporous carbon C-2 (morphology of C-1 is very similar to that of C-2). It can be seen that both the template and the carbon display a similar morphology made up of bundles of bamboo-shaped primary particles with a diameter of around 400 nm and a length of about 10 μm. Additionally, the low-magnification SEM image of C-2 shown in Figure 3d reveals that the carbon particles are segregated, indicating that conglutination

of the carbon particles did not occur during the CVD process. However, particle conglutination is a serious problem when a liquid carbon precursor is used.[35]

3.5. TEM Observation. The pore-structural features of sample SBA-15N and carbons C-1and C-2 can be seen from Figure 5. The images shown in parts a, b, and c of Figure 5 were taken along the [001] direction while the images shown in parts b, d, and f of Figure 5 were collected along the [100] direction. The presence of hexagonal mesoporous arrays of SBA-15N and the carbons is evidenced. The highly ordered arrays of the pore channels of both carbons can be clearly seen from parts c and e of Figure 5. The interplanar distance of C-1 and C-2 were estimated to be around 10 nm, in good agreement with the value determined from the SAXS data (see Table 1). The diameter of the carbon nanorods was estimated to be about 7 nm. According to a previous study,[33] the diameter of the carbon nanorods of a SBA-15-templated mesoporous carbon prepared with sucrose as the carbon precursor is about 7 nm. The authors observed a difference of 2.2 nm between the diameter of the carbon rods and the pore diameter of the template (9.2 nm), and attributed the difference to carbon shrinkage during carbonization. In the present work, the pore diameter of the template after thermal treatment at 900 °C was estimated to be about 7.2 nm, in a fairly good agreement with the diameter of the carbon nanorods (7.0 nm), suggesting a minor shrinkage of carbon when the CVD method is used. Similarly, the spacers, which are constituted by the carbon that filled the channel-interconnecting micropores of SBA-15,[33] also have a lower degree of carbon shrinkage, thus improving the mechanical stability of the templated carbon. In addition, the space between the carbon nanorods and pore channel walls of template is always found when using liquid carbon precursors due to the significant shrinkage of carbon nanorods. However, the nitrogen adsorption analysis of composite silica/carbon before washing with HF solution showed that no micropores and mesopores were observed in this work (not shown here), further demonstrating that the pyrolytic carbon was completely filled into the pores of template silica. A denser carbon layer on the external surface of carbon C-2 can be seen from Figure 5f. This nontemplated carbon layer was formed because of the prolonged CVD time employed in preparing carbon C-2. Such a nonporous carbon layer will cause the surface area and pore volume of carbon C-2 to be lower than that of carbon C-1 as shown by the data in Table 1.

Shown in Figure 6 are the lattice-fringe images of carbon C-2 taken along the long axis [001] direction (arrow direction in Figure 6a) and on the external surface (Figure 6b). The direction of stacked graphene sheets composed of carbon nanorods parallel to the [001] direction is different from what was observed by Yang et al.[10] or Kim et al.,[11] in which the orientation of the graphene sheets is perpendicular to the long axis of the carbon nanorods. The direction of stacked

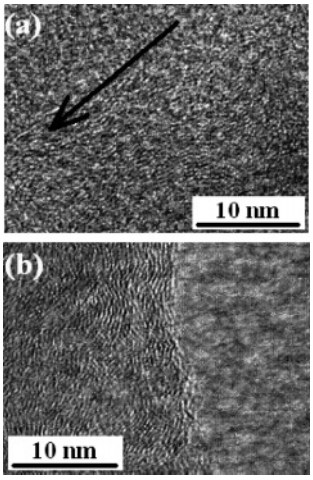

Figure 6. FETEM images of lattice fringe of carbon C-2 along the [001] direction (arrow direction) (a) and on the external surface (b).

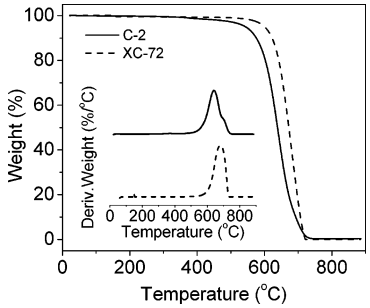

Figure 7. TG and DTG curves (inset) in air of carbon C-2 and carbon black XC-72.

graphene may have an influence on the electrochemical properties of carbon materials.[10] Figure 6b also shows that the discrete stacking graphene sheets of external carbon layer parallel to the external surface of template silica. It can be seen that the graphitic structure of internal carbon in Figure 6a seems little different from that of external carbon in Figure 6b possibly due to the confinement of template silica channels.

With consideration of the mechanism of carbon deposition using CVD in preparation of carbon molecular sieves,[18,36] the formation mechanism of the ordered graphitic mesoporous carbons prepared in this study is understood as follows. At 900 °C, the pyrolysis products of benzene have been observed to consist of polycyclic aromatic hydrocarbons such as biphenyl, *m*-, *p*-, and *o*-terphenyls, and anthracene, together with benzene.[18] It is believed that these organic species first chemically adsorb on the pore walls of the micropores of the template because of a stronger adsorption potential of smaller pores, then on the mesopore walls. Subsequently, aromatization and carbonization of the adsorbed organic species, catalyzed by surface isolated hydroxyl groups,[37] take place to form the first layer of graphitic pyrolytic carbon.[38] A layer-by-layer stacking mechanism by autocatalysis will follow up to create graphene sheets. Thus,

(33) Jun, S.; Joo, S. H.; Ryoo, R.; Kruk, M.; Jaroniec, M.; Liu, Z.; Ohsuna, T.; Terasaki, O. J. Am. Chem. Soc. 2000,122, *10712*.
(34) Xiong, Y.; Xie, Y.; Li, X.; Li, Z. *Carbon* **2004**, *42*, 1447.
(35) Kim, T. W.; Ryoo, R.; Gierszal, K. P.; Jaroniec, M.; Solovyov, L. A.; Sakamoto, Y.; Terasaki, O. *J.* Mater. Chem. **2005**, *15*, 1560.
(36) Kawabuchi, Y.; Oka, H.; Kawano, S.; Mochida, I.; Yoshizawa, N. *Carbon* **1998**, *36*, 377.
(37) Zhao, X. S.; Lu, G. Q.; Whittaker, A. J.; Millar, G. J.; Zhu, H. Y. *J. Phys. Chem. B* **1997**, *101*, 6525.
(38) Fitzer, E., Mueller, K.; Schaefer, W. *Chem. Phys. Carbon* **1971**, *7*, 237.

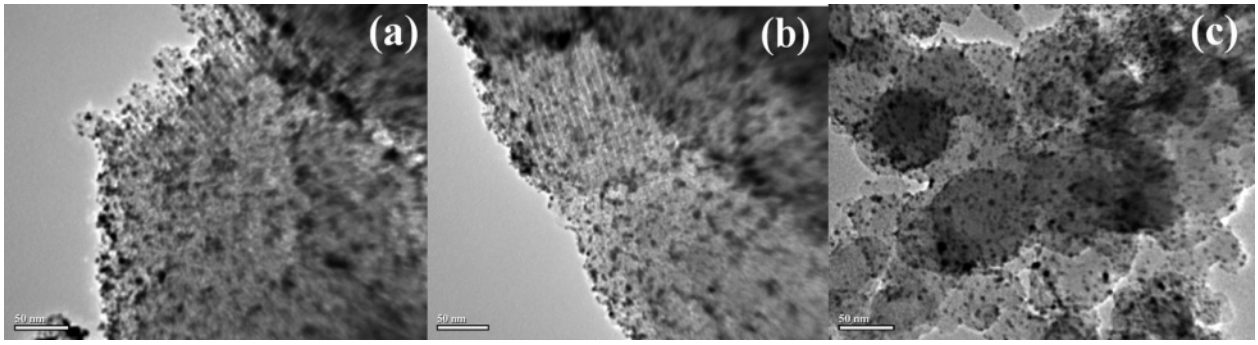

Figure 8. TEM images of catalysts Pt/C-1(a), Pt/C-2 (b), and Pt/C (E-TEK) (c).

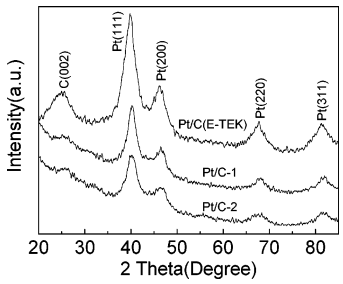

Figure 9. XRD patterns of Pt/C-1, Pt/C-2, and Pt/C (E-TEK) catalysts.

the direction of stacked graphene sheets composed of carbon nanorods is parallel to the long axis of the nanorods. Carbon deposition in the template pores will stop when the pore size becomes smaller than the kinetic size of benzene molecule (0.36 nm).[18,36] As a result, further carbon deposition will occur on the external surface of the template, forming a layer of dense carbon as revealed by the SEM image shown in Figure 5f. Thus, precise control over CVD time may allow one to reduce the external carbon layer or even though create carbon nanopipes instead of nanorods while the use of a higher CVD temperature may produce a higher degree of graphitic carbon.[22] Our further study has partially demonstrated this proposed mechanism and will be given in great detail in another work. It should be noted that the CVD mechanism proposed here is different from that proposed by Mokaya et al.,[22,26,27] in which the authors suggested that a carbon precursor is first in contact with the outer surface of SBA-15 silica before diffusing into the interior of the silica, and the deposited carbon may block the pore channels and hinder access of carbon precursor to the core of the silica particles. Thus, removal of template resulted in a mesoporous carbon with a hollow core and ordered shell structure.[22,26]

3.6. Thermogravimetric Analysis. Figure 7 shows the thermogravimetric behaviors of carbon C-2 and carbon black XC-72 in air. The thermogravimetric behavior of C-1 is similar to that of C-2 (not shown here). The key message from the TGA curves shown is that the silica template had been completely dissolved away by the aqueous HF solution because of the illegible residue at 800 °C of carbon C-2. The DTG curve (inset) of carbon C-2 displays a similar weight-loss profile to that of carbon black XC-72. The significant weight losses of C-2 occurred in the temperature range of 550−740 °C, which is higher than that of a graphitic mesoporous carbon templated from SBA-15 using aromatic acenaphthene as a carbon precursor,[11] in which the oxidation of graphitic carbon in air was found to be in the range of 520−680 °C. Our observation of the oxidation temperature range of graphitic carbon is comparable to that of impurity-free single-walled carbon nanotubes (550−750 °C),[20] further demonstrating that obtained carbon consists of graphitic carbon with a high thermal stability.

3.7. Pt Catalysts Supported on Carbon. Figure 8 compares the TEM images of catalysts Pt/C-1, Pt/C-2, and Pt/C (E-TEK). It can be estimated that the particle sizes of the Pt catalysts supported on carbons C-1 and C-2 are larger than that of catalyst Pt/C (E-TEK). Figure 9 shows the XRD patterns of the three Pt catalysts. It should be noted that the peak at about 25° is due to the (002) diffraction of the graphitic carbon. The diffraction peaks at the Bragg angles of 39, 46, 67, and 81° correspond to the (111), (200), (220), and (311) facets of Pt nanocrystals.[39] The average Pt particle sizes of catalysts Pt/C (E-TEK), Pt/C-1, and Pt/C-2 calculated using Scherrer's equation based on the Pt (111) peak are 3.5, 5.3, and 5.4 nm, respectively, which are consistent with the TEM observations. The different Pt particle sizes are believed to be due to the different surface chemistries of the carbon supports.[40]

3.8. Electrochemical Properties. Figure 10a shows the cyclic voltammograms (the current has been normalized to the geometric surface area of the working electrode) of catalysts Pt/C-1, Pt/C-2, and Pt/C (E-TEK) in 0.5 M H_2SO_4. The observed hydrogen adsorption/desorption peaks in the potential range of −0.2 V to 0.1 V are because of the presence of different Pt facets, which are also shown in the XRD data. The electrochemically active surface areas of the Pt catalysts can be estimated from the charges associated with hydrogen adsorption on Pt facets. It can be seen that the electrochemical surface area for Pt/C-1 and Pt/C-2 is smaller than that of catalyst Pt/C (E-TEK). Because of the smaller Pt particle size and higher graphitic crystallinity of catalyst Pt/C (E-TEK) than catalysts Pt/C-1 and Pt/C-2, its mass activity (35 mA/cm^2) (normalized to the geometric surface area of the working electrode) for room-temperature methanol oxidation is higher than that of Pt/C-1 (19 mA/cm^2) and Pt/C-2 (15 mA/cm^2).

However, catalysts Pt/C-1 and Pt/C-2 displayed a higher specific activity than catalyst Pt/C (E-TEK) did as can be seen from Figure 10b. Here the specific activity was evaluated by using the current value of the peak at about 0.65 V, which is an indication of the intrinsic activity of Pt

(39) Li, W.; Liang, C.; Zhou, W.; Qiu, J.; Zhou, Z.; Sun, G.; Xin, Q. *J. Phys. Chem. B* **2003**, *107*, 6292.
(40) Chan, K.-Y.; Ding, J.; Ren, J.; Cheng, S.; Tsang, K. Y. *J. Mater. Chem.* **2004**, *14*, 505.

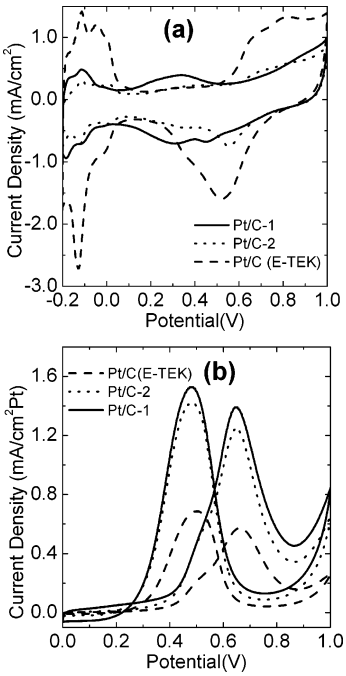

Figure 10. Cyclic voltammograms of Pt/C-1, Pt/C-2, and Pt/C (E-TEK) catalysts measured at a scan rate of 20 mV s^{-1} at room temperature in electrolytes of (a) 0.5 M H_2SO_4 and (b) 1 M CH_3OH + 0.5 M H_2SO_4.

sites. It is seen that the specific activities of catalysts Pt/C-1 and Pt/C-2 are 1.39 and 1.25 mA/cm^2 Pt, respectively. However, the specific activity of the commercial catalyst, Pt/C (E-TEK), is about 0.57 mA/cm^2 Pt. Therefore, Pt catalyst supported on carbons C-1 and C-2 is catalytically more active than those supported on XC-72. The presence of ordered mesopores of carbon supports C-1 and C-2 may also contribute to the observed higher specific activity because of the facile transport of methanol and the oxidation products in these ordered pores.[41]

4. Conclusions

In summary, the experimental results presented in this paper have demonstrated that mesoporous pure silica SBA-15 without loading any catalytic component can be used as a template to fabricate ordered mesoporous carbon with graphitic pore walls using gaseous benzene carbon precursor via a CVD process. The CVD method affords little shrinkage of carbon framework. By controlling CVD time, one can avoid the formation of a dense carbon layer on the external surfaces of the template particles. The direction of stacked graphene sheets composed of carbon nanorods was observed to be parallel to the long axis of the nanorods. The specific activity of Pt catalyst supported on the template-synthesized carbon materials outperforms a commercial catalyst, Pt/C (E-TEK), for room-temperature methanol oxidation.

Acknowledgment. We thank NUS for financial support (Grant Number R279000124112). We also thank Dr. Li Xu for SAXS measurement, Dr. Xu Xiaojing and Mr. Shang Zhenhua for TEM measurement, and Prof. Shen Zexiang for the measurement of Raman spectra.

CM0502222

(41) Chai, G. S.; Shin, I. S.; Yu, J. S. *Adv. Mater.* **2004**, *16*, 2057.